Received 12 September 2022; revised 15 March 2023; accepted 24 March 2023. Date of publication 28 March 2023; date of current version 6 April 2023.

Digital Object Identifier 10.1109/OJAP.2023.3262698

Systematic Design Method for Mutual Coupling Reduction in Closely Spaced Patch Antennas

HUI DENG (Graduate Student Member, IEEE), LEI ZHU (Fellow, IEEE), AND ZHAO-AN OUYANG (Member, IEEE)

Department of Electrical and Computer Engineering, Faculty of Science and Technology, University of Macau, Macau, China

CORRESPONDING AUTHOR: L. ZHU (e-mail: leizhu@um.edu.mo)

This work was supported in part by the National Natural Science Foundation of China under General Program under Grant 61971475; in part by the Science and Technology Development Fund of Macao under FDCT Research under Grant 0085/2020/AMJ, Grant 0095/2019/A2, and Grant 0080/2021/A2; and in part by the University of Macau under Special Grant CPG2022-00008-FST.

ABSTRACT In this article, a systematic design approach is presented to reduce the mutual coupling between a pair of closely spaced microstrip patch antennas (MPAs). This method can effectively overcome the main drawback of previous two-path cancellation methods, i.e., lack a systematic design guideline and heavily rely on the time-expensive trial-and-error procedure to mitigate mutual coupling in a best-effort manner. To this end, we first propose the concept and workflow of the systematic design method, and introduce the circuit-level modeling upon the proposed two coupling routes. Then, prototyped on a practical and simple physical structure, we perform certain accurate extractions and derive the rigorous conditions for both of isolation between two patches and impedance matching of a single patch based on these two paths. Afterwards, according to the circuit-level discussion on lumped elements, the corresponding decoupling structure could be implemented substantially and designed quantitatively at the antenna level for particularized closely spaced MPAs. Finally, a prototype is simulated, fabricated, and measured to validate the proposed method. The results show that the circuit-model calculation, full-wave simulation, and measurement are in good agreement. By virtue of such a simple decoupling structure, the poor 7-dB isolation is dramatically improved to 58 dB, and the isolation is enhanced beyond 20 dB in the entire impedance matching bandwidth range of 4.38 $\sim$ 4.60 GHz (4.9%), with the closely center-to-center spacing of 0.37 λ_0.

INDEX TERMS Closely spaced patch antennas, decoupling, multiple-input multiple-output (MIMO) antenna, mutual coupling, systematic design method.

I. INTRODUCTION

IN RECENT years, multiple-input and multiple-output (MIMO) antenna systems have become more and more prevalent in various modern wireless communication systems due to the benefits of improved spectrum utilization and enhanced channel capacity. With the growing demands for flexibility and high throughput in wireless systems, it makes sense to reduce the size of the antennas arrays used in MIMO systems [1], [2]. However, severe correlation and mutual coupling will inevitably occur between the close spacing of antenna elements, which unfortunately compromises the performance of MIMO systems [3]. On the other hand, since the intrinsic advantages of low profile, lightweight, and ease of integration, microstrip patch antennas (MPAs) have been regarded as an increasingly popular form of the antenna element in MIMO systems. In light of this, it is highly urgent and significant to find a simple, effective, and design-friendly method to reduce the mutual coupling between the closely spaced patch antennas.

Thus far, one well-established technique mainly focuses on introducing a variety of isolation elements between the radiators to block the surface current or near-field coupling directly, such as electromagnetic band-gap (EBG) structures [4], [5], [6], split-ring resonators (SRR) [7], polarization-conversion isolators (PCI) [8], dielectric block [9], coupling-mode transducers [10], defected ground structures (DGS) [11], and meta-structure wall [12], [13]. However, most of the mentioned decoupling structures or techniques usually suffer from complicated geometry, high profile, and deteriorated radiation performance. The central arrangement of decoupling structures is also unsuitable for closely spaced arrays.

Another category of technique is introducing a decoupling and matching network (DMN) between the antenna elements and the actual input ports to achieve isolation and matching in circuit characteristics [14], [15], [16]. The separated networks facilitate the design analytically and systematically, but yield ohmic losses as demonstrated and require occupying additional spaces, e.g., multiple layers and overall footprint [17]. Besides, superimposing different modes or electric fields to eliminate the total electric fields at the input ports could also be used to reduce mutual coupling. In [18], [19], [20], [21], a pair of hybrid modes, eigenmodes, and specific in-set feeding ports of the MPAs were utilized skillfully, respectively, so that the mutual coupling can be suppressed without additional structures. Most of them tend to modify the patch elements heavily and lack systematic guidance. This hurdle has been settled in [22] based on the even-odd characteristic modes method, but it is only applicable under a single patch so far. In [23], a distributed inductance was introduced between the antenna elements and designed based on the common mode and differential mode (CM/DM) cancellation theory, but the limited level of decoupling prevents its application to some highly isolated scenarios [24], [25].

Very recently, a decoupling structure composed of a microstrip line and a shorting pin is presented in [26] to reduce the mutual coupling between closely coupled MPAs in H-plane. Compared with other works that introduce an extra coupling path to eliminate the original coupling path, such as the microstrip U-section [27], array-antenna decoupling surface (ADS) [28], and neutralization lines (NL) [29], the skillfully sided arrangement makes this scheme more appropriate for closely spaced MPAs. Unfortunately, constrained by the fact that the two paths cannot be separated independently and invisible, the only qualitative design guideline could be presented under the assumption that the two coupling paths are equally amplitude but out of phase. As such, these existing two-path cancellation efforts are unfortunately faced with the design-unfriendly dilemma, that is, impedance matching and mutual coupling reduction can be only achieved in a best-effort manner via trial and error during the design process, which would waste a lot of time on simulation or optimization.

In this article, a systematic design approach is proposed to reduce the mutual coupling between two closely spaced MPAs. This concept is inspired by the classical filtering antenna work [30] and introduced to address two major challenges, i.e., 1. A quantitative design guideline is presented to significantly reduce the design complexity under two-path decoupling; 2. The isolation performance is analyzed and predicted theoretically to exploit the potential of the decoupling structure more effectively. In the remainder if this article, Section II describes the concept of the systematic design method, perform the circuit-level accurate modeling, and derive the conditions of high isolation between two closely spaced patches and good impedance matching of each patch. According to the theoretical investigation at the circuit level, the design and implementation at the antenna level are illustrated in detail in Section III. Section IV gives the experimental validation. The measured results demonstrate that excellent isolation performance, sufficient operating bandwidth, and improved radiation performance are all achieved solely with a very simple decoupling structure. Finally, the conclusion is given in Section V.

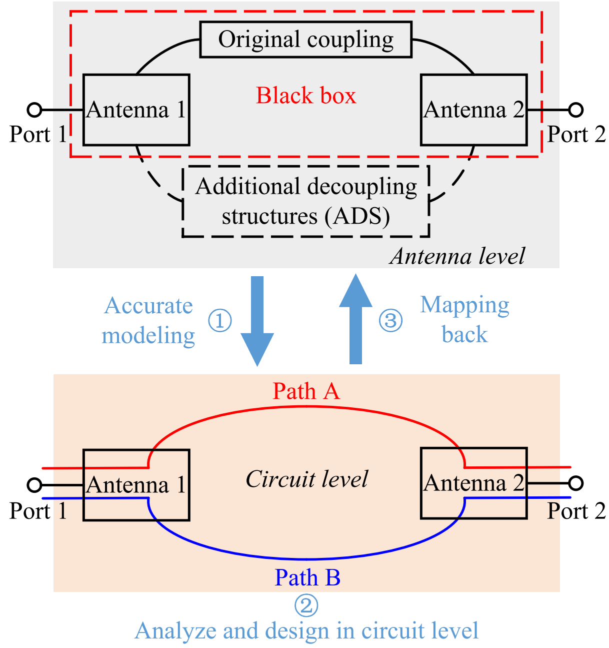

FIGURE 1. Topology of the proposed systematic design method for the mutual coupling reduction in closely spaced MPAs.

II. SYSTEMATIC DESIGN METHODOLOGY

The topology of the proposed systematic design method for the mutual coupling reduction in closely spaced patch antennas is depicted in Fig. 1. Traditional decoupling design approaches mainly focus on the antenna level, with the concept of introducing and designing an additional decoupling structure (ADS) to mitigate the isolation between the two patch antennas in a best-effort manner. A few works have also tried to use equivalent circuits to help better explain the decoupling principle [31], [32], [33]. However, it is known that the antenna-level design method only establishes the relationship between the additional decoupling structure and the scattering parameters of the input ports, while the original coupling between the antennas becomes a neglected black box and its performance is hardly analyzed. In this context, only qualitative analysis and design can be realized on the antenna level, but not a systematic quantitative design. To address this technical challenge, we additionally introduce a circuit-level

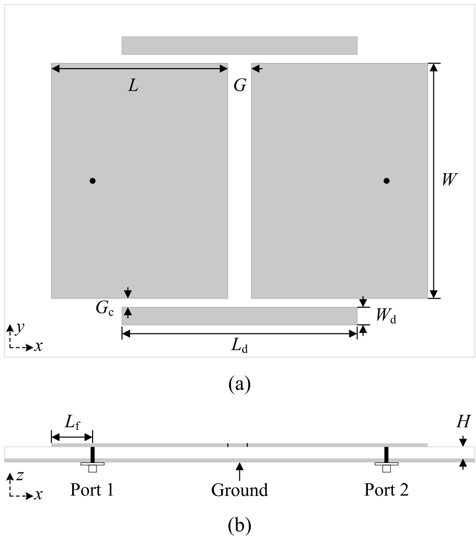

FIGURE 2. Schematic diagram of the closely spaced MPAs with the proposed decoupling structure. (a) Top view. (b) Side view. The dimensions of the radiating patch are $W = 30$, $L = 21.5$, $H = 3.5$, $G = 3$, $L_d = 28.7$, $W_d = 2$, $G_c = 0.5$, $L_f = 2.75$ (Unit: mm), and the relative permittivity of the substrate is $\varepsilon_r = 2.2$.

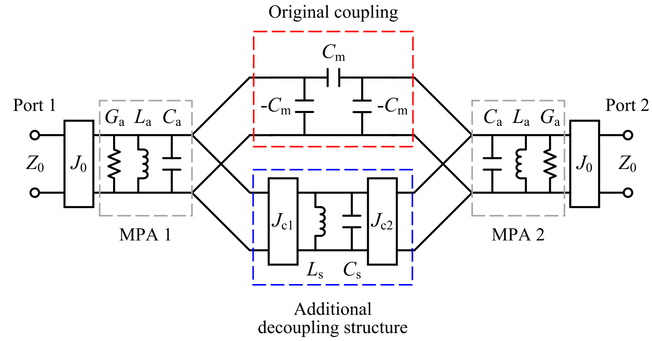

FIGURE 3. Corresponding equivalent model at the circuit level of the entire structure in Fig. 2.

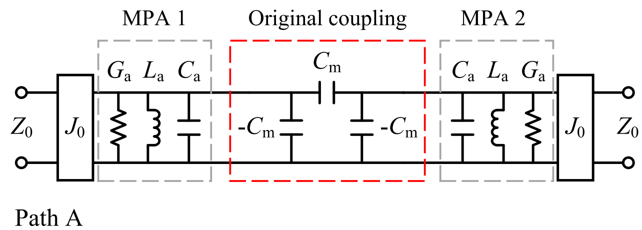

FIGURE 4. Equivalent circuit model of the original coupling path.

modeling during the analysis and design procedure so that the two paths (Path A and Path B) become intuitively visible and they can be analyzed independently, and then map the circuit-level investigation back to the antenna level to achieve a systematic design. The detailed workflow is illustrated as:

Step 1: Accurately model the antenna coupling path (Path A). The original coupling between the radiating patches needs to be extracted precisely;

Step 2: The path of the antenna through the additional decoupling structure (Path B) is accurately modeled; (The above two steps correspond to Stage 1 in Fig. 1)

Step 3: Analyze the relationship between the two paths at the circuit level to obtain the isolation conditions and the quantitative relationship between the circuit components of the two paths;

Step 4: Analyze the impedance matching conditions at the circuit level to obtain the constraints and design goals; (These two steps correspond to Stage 2 in Fig. 1)

Step 5: Complete the physical design at the antenna level by using the mapping relationship between the circuit models and the dimensional parameters, as well as the above isolation and impedance matching conditions. (This step corresponds to Stage 3 in Fig. 3 and will be illustrated in detail in Section III.)

Fig. 2 depicts a simple and practical example for further illustrating the concept of the proposed systematic design method, which consists of two identical rectangular patches arranged in an E-plane coupled manner and two identical side-by-side arrangement half-wavelength microstrip lines. The two closely spaced patches are fed by two coaxial probes placed along the central axis, respectively. The corresponding equivalent model at the circuit level of the entire structure is shown in Fig. 3, and its detailed modeling procedure is described as below.

A. ACCURATE MODELING FOR TWO PATHS: PATH A

Firstly, the equivalent circuit model of the original coupling path (Path A) is depicted in Fig. 4, which is modeled as follows. The two parallel *GLC* circuits are used to equivalently model the two identical patch radiators, where the values (G_a, L_a, and C_a) can be calculated analytically under a single patch based on the classical cavity model theory [34] or the extraction approach reported in work [35]. The admittance-inverter (J_0) is employed to represent the external coupling between the input port and the patch antenna, which is replaced here by a parasitic series inductance (L_p) due to the probe feeding. As for the mutual coupling between the two radiated patches, it is modeled as a capacitive π-network with the value of C_m. Obviously, C_m is the crucial parameter of this equivalent circuit, which can be calculated by [36]

$$C_m = CC\sqrt{C_a C_b} \tag{1}$$

where $C_a = C_b$, and CC is the coupling coefficient between the two radiating patches as can be calculated by (13) and (14) in the Appendix, where details of the extracted method and their derivations are also provided.

According to the dimensions of the patch radiators listed in the caption of Fig. 2, the corresponding lumped elements are calculated to be $G_a = 7.41$ mS, $L_a = 0.48$ nH, $C_a = 3.28$ pF, and $L_p = 2.59$ nH. C_m is easily determined to be 0.28 pF based on (1), (14), and the two frequencies (f_1 and f_2) from the S_{21} magnitude response are shown in Fig. 5. As such, the calculated S-parameters of Path A can be derived as depicted in Fig. 6, which are in general agreement with the full-wave simulation results within the impedance matching bandwidth of the single patch antenna (about 5% theoretically). The slight out-of-band inconsistency is mainly caused by minor

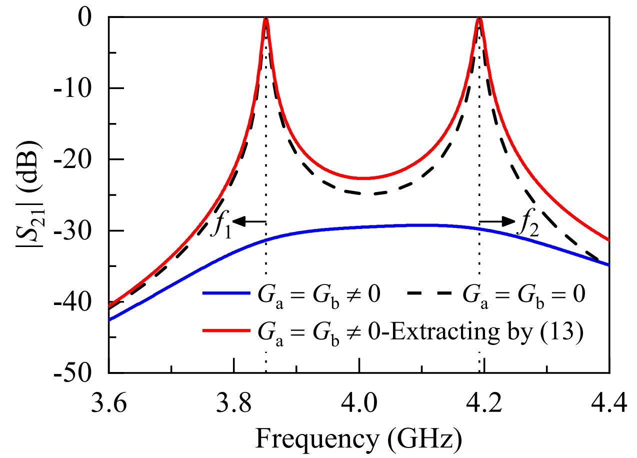

FIGURE 5. Post-processing procedure under weak external coupling for extraction of the coupling coefficients and corresponding C_m from the two radiating MPAs, supposing a fixed $G = 3$ mm.

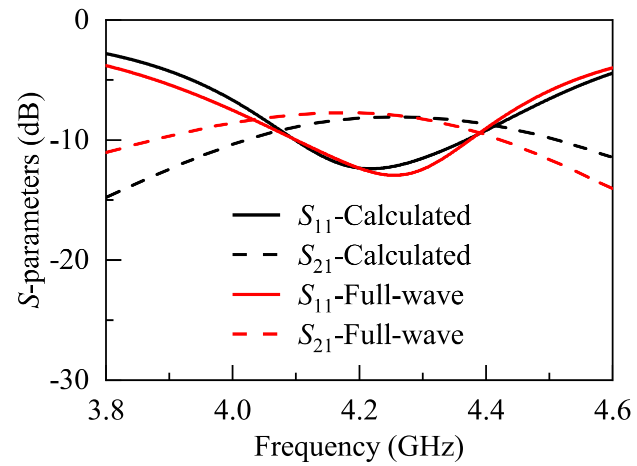

FIGURE 6. Calculated and full-wave simulated S-parameters of Path A.

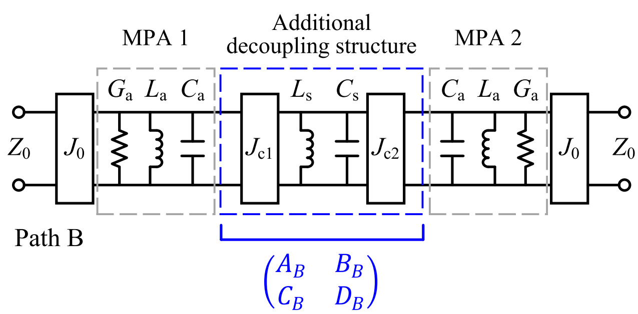

FIGURE 7. Equivalent circuit model of the additional coupling path.

resistive coupling, but it hardly affects the actual accuracy in analysis of in-band decoupling and thus it can be fully neglected in the modeling [37].

B. ACCURATE MODELING FOR TWO PATHS: PATH B

Subsequently, the equivalent circuit of the additional coupling path (Path B) is modeled and depicted in Fig. 7. The modeling of the two radiating patches is the same as that in Path A. A parallel LC circuit is used to model the open-circuit half-wavelength microstrip line, whose values (L_s and C_s) can be calculated based on the closed-form expressions in [38]. Specifically, the characteristic impedance in the formulas also can be readily obtained with the help of some transmission line tools. The admittance-inverters (J_{c1} and J_{c2}) represent the coupling extent between the two radiating patches and the non-radiative half-wave microstrip line, respectively. Their values can be determined as follows: using the method reported in work [39] to extract the coupling coefficient and then employing the relationship between J-inverter and the coupling coefficient to calculate and determine [40].

Since the overall structure of the two closely spaced patch antennas is geometrically symmetric with respect to the yoz plane, the absolute values of the extracted coupling coefficients are the same but with the opposite signs, that is, $J_{c1} = -J_{c2} = J_c$. The minus sign is caused by the microstrip line operating in the half-wave mode with opposite electric fields on two sides, and it can be deduced from the coupling coefficient as defined in [41]. Furthermore, the additional decoupling section (framed by the blue dashed line) can be regarded as a unity and is derived as

$$\begin{pmatrix} A_B & B_B \\ C_B & D_B \end{pmatrix} = \begin{pmatrix} 0 & -\frac{j}{J_{c1}} \\ -jJ_{c1} & 0 \end{pmatrix}\begin{pmatrix} 1 & 0 \\ j\omega C_s + \frac{1}{j\omega L_s} & 1 \end{pmatrix}\begin{pmatrix} 0 & -\frac{j}{J_{c2}} \\ -jJ_{c2} & 0 \end{pmatrix}$$
$$= \begin{pmatrix} -\frac{J_{c2}}{J_{c1}} & -j\omega\frac{C_s - \frac{1}{\omega^2 L_s}}{J_{c1}J_{c2}} \\ 0 & -\frac{J_{c1}}{J_{c2}} \end{pmatrix} \quad (2)$$

When substituting $J_{c1} = -J_{c2} = J_c$ into (2) and simplifying, it is unexpectedly found that this A-matrix has the same form as a series inductance, such that

$$L_m = \frac{1}{{J_c}^2}\left(C_s - \frac{1}{\omega^2 L_s}\right) \quad (3)$$

This means that the mutual coupling in Path B and Path A constitutes a duality. Herein, the $\omega = 2\pi f$ in (3) is actually the desired frequency for realization of excellent decoupling, and not the resonant frequency (f_s) of the half-wave microstrip line. In contrast, if $f = f_s$, there is $L_m = 0$, implying that no coupling is present in Path B or Path B fully disappears. This is a completely different conclusion as derived from the qualitative analysis that a parasitic half-wave resonator operates at the isolated frequency in other relevant works.

C. CONDITION FOR ISOLATION

Till now, the two coupling paths are successfully separated and independently visible based on the accurate equivalent circuit model mentioned above. Path A and Path B could be regarded as two second-order lossy bandpass filter with electric and magnetic coupling, respectively. Thus, it can be assumed that the equivalent coupling lumped elements in the combined paths satisfy [41]

$$L_m = L_a\frac{C_a}{C_m} \quad (4)$$

When substituting (3) into (4) and simplifying, it is yielded

$$J_c = \sqrt{C_m\left(C_s - \frac{1}{4\pi^2 f^2 L_s}\right)/(C_a L_a)} \tag{5}$$

where C_s and L_s can be further mapped to the physical decoupling structure and predetermined based on the quasi-static theory of microstrip line structure, thus yielding

$$C_s = \frac{L_d\sqrt{\varepsilon_e}}{2cZ_s} \tag{6a}$$

$$L_s = \frac{2L_d Z_s\sqrt{\varepsilon_e}}{c\pi^2} \tag{6b}$$

where ε_e is the effective permittivity, c is the speed of light in free space, and Z_s is the characteristic impedance depending on W_d and H, and L_d is the physical length of the microstrip line.

As demonstrated in (5) and (6), the coupling coefficient between the radiating patch and the decoupling structure could be quantitatively calculated at the operating frequency after the mutual coupling between the specified closely spaced MPAs is determined. Thus, a set of lumped-element values (L_s = 1.5 nH, C_s = 1.65 pF, and J_c = 0.01 S) in Path B are obtained accordingly based on the extracted and calculated values of Path A in Section II-A.

Then, the transmission characteristics of the two paths and the total path are calculated using the prescribed variables and eventually depicted in Fig. 8. Herein, although the resonator loss (insertion loss) denoted by G_a does not affect the mutual coupling as proved in Fig. 5, it does have any significant effect on the port impedance matching (external quality factor), which will indirectly distort the transmission response. Hence, the transmission responses discussed below are initially in the lossless case ($G_a = 0$). As shown in Fig. 8(a), both paths present a typical response of the second-order bandpass filter with a staggering frequency (seeing in the inset). Within the band of interest, the amplitudes of the two paths partially overlap, as can be intuitively seen from the magnitude ratio (S_{21}^a/S_{21}^b). Meanwhile, the phase difference ($\phi_{21}^b - \phi_{21}^a$) of the two paths is determined by the staggering passband frequency, which shows a 180° out of phase at f_z. As such, the transmission response of the total path is plotted in Fig. 8(c), which shows a corresponding typical zero-point response at f_z. When the radiation loss is considered, the total transmission response also produces a zero point at f_z as previously exhibited, and the amplitude decreases in the nearby frequency band. Therefore, these results demonstrate indeed that, at the proposed circuit level, the transmission coefficient (mutual coupling) between the two ports could be reduced effectively over a certain range of bandwidth with our well-performed modeling investigations.

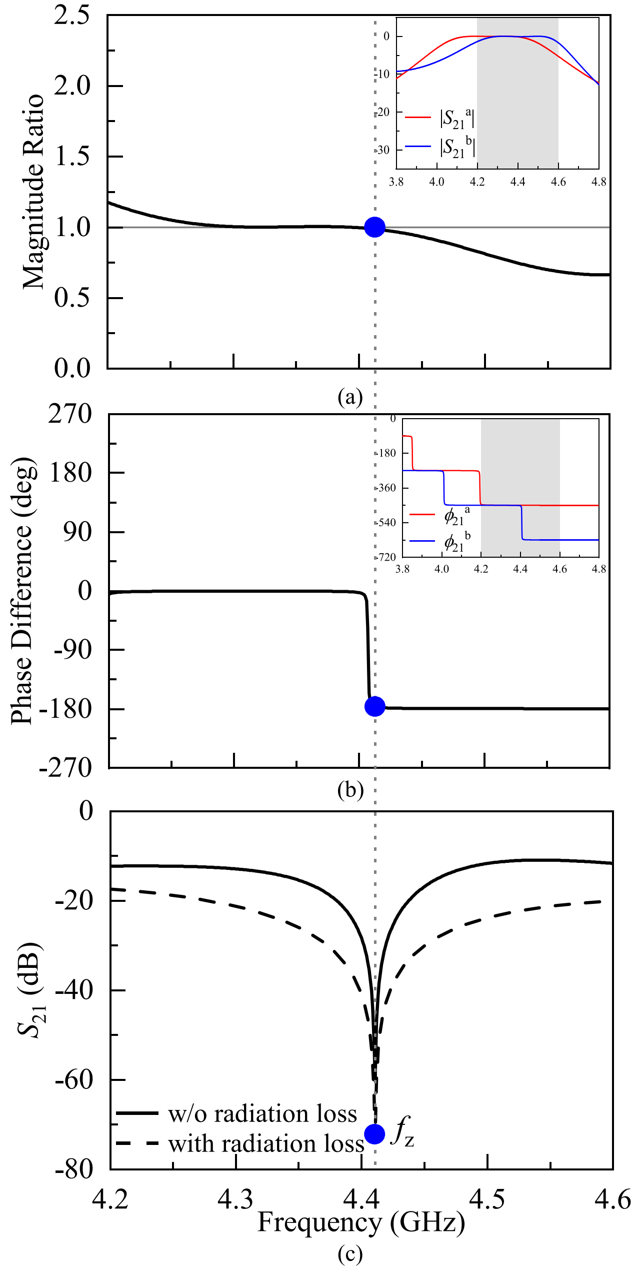

FIGURE 8. Theoretical transmission characteristics of the two separated paths and the total path based on the circuit models. (a) Magnitude ratio. (b) Phase differences. (c) Predicted transmission coefficients of the total path.

D. CONDITION FOR IMPEDANCE MATCHING

The impedance matching is another issue that needs to be addressed in addition to the concerned isolation, which can characterize a passband transmission response between the input port and the radiation conductance. To remove the interference caused by the transmission responses between the two ports, port 2 is set as an open-circuit. The input admittances and reflection coefficients looking into from port 1 for two separated paths and the total path are calculated and depicted in Fig. 9. As seen, Path A and Path B have the smallest reflection coefficients at f_{pa} and f_{pb}, respectively, while the best matching point for the total path is located between them. This is because when the coupling of Path B is introduced to mitigate Path A, the total input conductance will gradually shift from Y_{ina} to Y_{inb}, as illustrated in Fig. 9(a). Therefore, the frequency (f_p) at

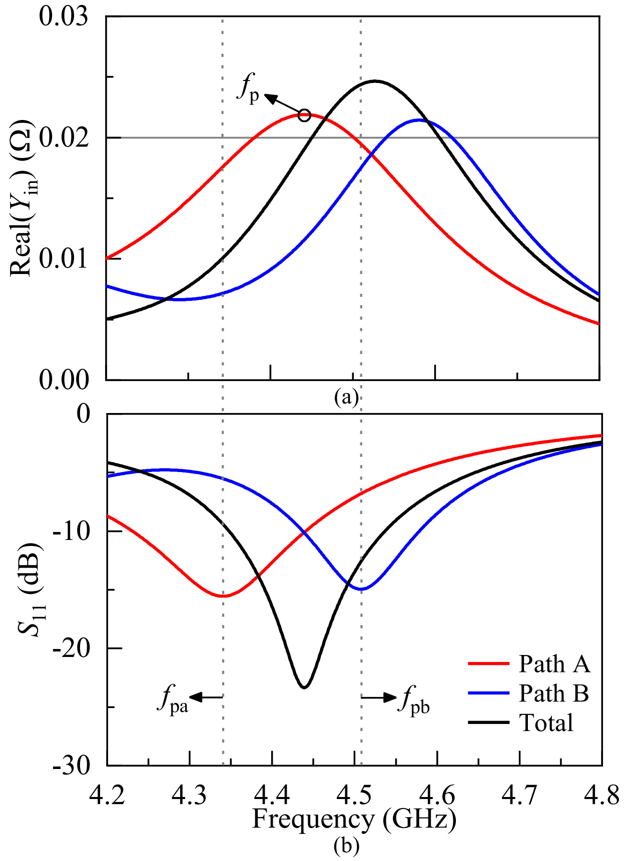

FIGURE 9. (a) Input admittances and (b) reflection coefficients looking into from port 1 for two separated paths and the total path.

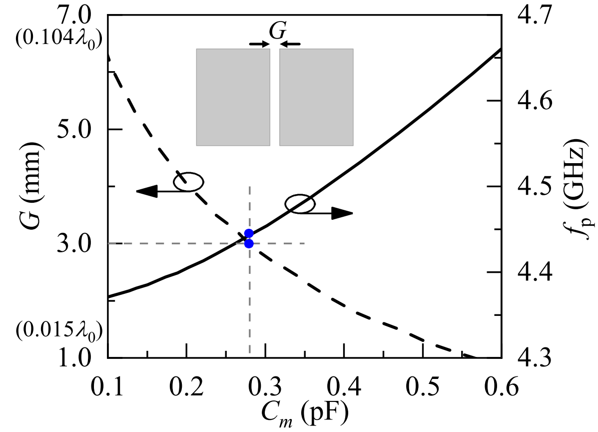

FIGURE 10. Extracted and calculated coupling capacitance between two patches at different spacing, and corresponding desired decoupling frequencies.

the input conductance peak of Path A could be chosen as the desired frequency for decoupling design (i.e., let $f_z = f_p$), and the input ports will be well-matched naturally when the mutual coupling is suppressed effectively. Most importantly, the above design step of pre-determining the impedance matching frequency greatly simplifies the design complexity, so there is no need to perform further impedance matching procedure by modifying the feeding structure or conducting the parameter study of the decoupling structures.

III. IMPLEMENTATION AND ACTUAL DESIGN

The physical implementation of reducing mutual coupling between a pair of closely spaced MPAs at the antenna level is presented in this section. Based on the discussion at the circuit level in Section II, the rigorous relationship of the lumped elements in the equivalent circuit models for decoupling and impedance matching was successfully obtained. Therefore, for closely spaced MPAs with determined parameters, the dimensions of the corresponding decoupling structures can be synthetically designed through parameter extraction and physically mapping to the dimensional layout. The EM simulation throughout this work is done by using ANSYS high-frequency structure simulator.

A. COUPLING COEFFICIENT BETWEEN TWO CLOSELY SPACED MPAS

In this design, the dimensions of the single MPA and the substrates are the same as those in Section II. Using the extraction technique proposed in the Appendix, the coupling coefficients between the two radiating patches at different edge-to-edge spacing can be easily obtained. Substituting them into (1), the relationship between the coupling capacitance (C_m) and the variation of spacing (G) is calculated and plotted in Fig. 10, which shows that the C_m gradually increases as the G decreases. Then, the desired decoupling frequency (f_p) corresponding to different spacings is calculated by substituting different C_m into the equivalent circuit of Path A. When $G = 3$ mm (corresponding to 0.04 λ_0 edge-to-edge spacing, 0.37 λ_0 center-to-center spacing, and maximum coupling of -7 dB) is chosen as the target for decoupling, $C_m = 0.28$ pF and $f_p = 4.45$ GHz can be conveniently determined from Fig. 10. In this context, the transmission responses of the total path at different J_c are investigated and calculated at the circuit level using (5) in Section II-C. As shown in Fig. 11, as J_c increases from 0.004 S to 0.016 S, the in-band isolation near the zero point of this closely spaced patch array gradually increases as well. In particular, when $J_c \geq 0.008$ S, S_{21} is less than -20 dB in the range of 4.33 $\sim$ 4.7GHz (8.2%), which is larger than the impedance matching bandwidth (5.2%) that is theoretically achieved by this MPA (denoted by grey region) [42].

B. COUPLING BETWEEN RADIATING PATCH AND DECOUPLING PART

According to the extraction method in previous work [39] and (5), (6) in Section II-C, the relationship between the coupling coefficients J_c and the physical parameters of the decoupling structure can be conveniently obtained. As shown in Fig. 12, as the gap (G_c) between the radiating patch and the half-wave microstrip line varies from 0.1 to 5 mm, J_c decreases gradually under different widths (W_d) and lengths (L_d) of the microstrip line. Considering the fabrication accuracy and

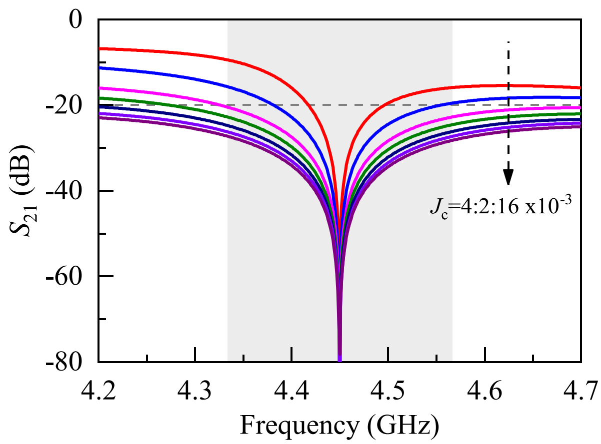

FIGURE 11. Transmission responses of the total path at different J_c.

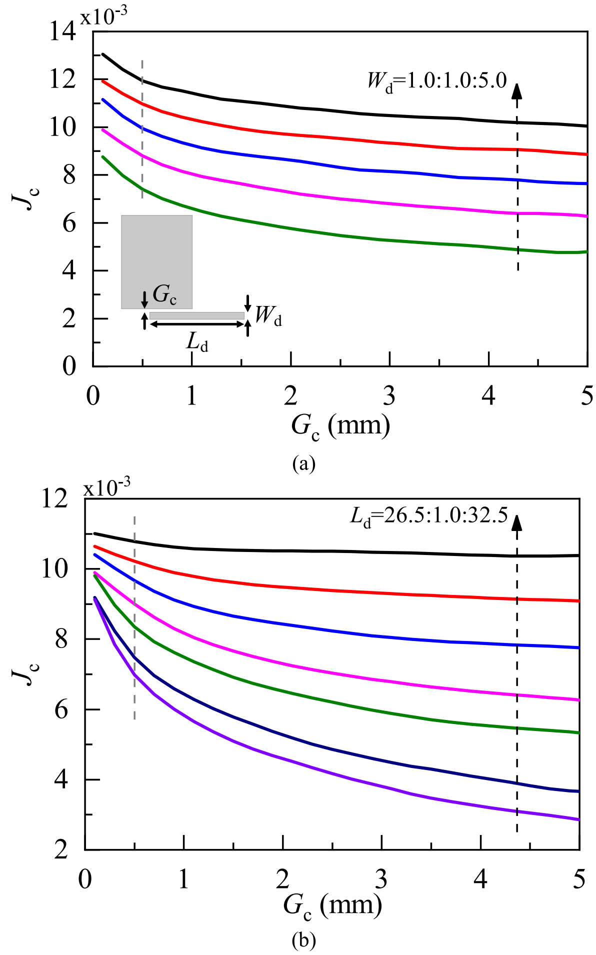

FIGURE 12. Extracted coupling coefficients between the patch and the microstrip line under different (a) widths, and (b) lengths.

geometrical compactness in practice, $G_c = 0.5$ mm and $W_d = 2$ mm are selected first, corresponding to $J_c = 0.0085$ S, which is enough for a 20-dB in-band isolation bandwidth. With the same J_c, L_d can be determined at around 28.5 mm, corresponding to the values of lumped elements of $C_s = 1.11$ pF and $L_s = 1.64$ nH. These dimensional parameters from the

TABLE 1. Comparison of the computation time.

Method	Total Number of Combinations	Computation Time	Reusable of Computations
Conventional	1287	6h 34m 11s	NO
Proposed	1287	3h 39m 54s	YES

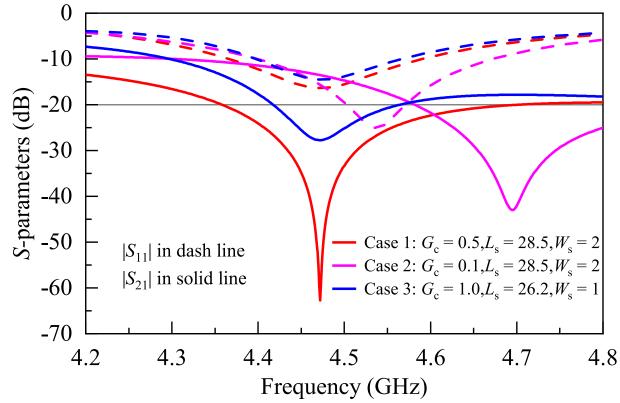

FIGURE 13. Simulated *S*-parameters of the proposed closely spaced MPAs under different dimensions of decoupling structures.

extraction will be used in the subsequent simulation and fabrication of the prototype.

In addition, the impact of the distance (G_c) between the decoupling structures and the patch antenna on decoupling performance is investigated. Three cases under different G_c are depicted in Fig. 13. Compared to case 1, when only G_c is changed, it is seen that case 2 cannot achieve decoupling effectively and the operating frequency also deviates from the expectation. Then, when increasing G_c along with adjusting other parameters to achieve decoupling within the desired operating band, it is found that the 20-dB isolation bandwidth is degraded. Therefore, G_c not only influences the isolation effectiveness but also has impacts on the isolation bandwidth.

Herein, the above cases also demonstrate that the parameters of the decoupling structure are usually dependent on each other and cannot be analyzed independently, which will severely increase the computations of the conventional method. As shown in Table 1, under the same parametric combinations, the proposed method significantly improves the design efficiency, saving nearly half of the computation time. Most importantly, the computations of the proposed method can be reused when the spacing or the desired isolation is changed.

IV. EXPERIMENTAL VERIFICATION

A. SIMULATED AND MEASURED RESULTS

In order to verify the validity of the proposed systematic design method, a prototype based on the extracted parameters is designed, simulated, and fabricated. The proposed closely spaced MPAs and the decoupling structures are printed on an F4B substrate with the relative permittivity of 2.20 and the loss tangent of 0.002. Two rectangular patches are excited directly by 50-Ω SMA probes. Based on the previous predetermined, the actual length of the decoupling structure

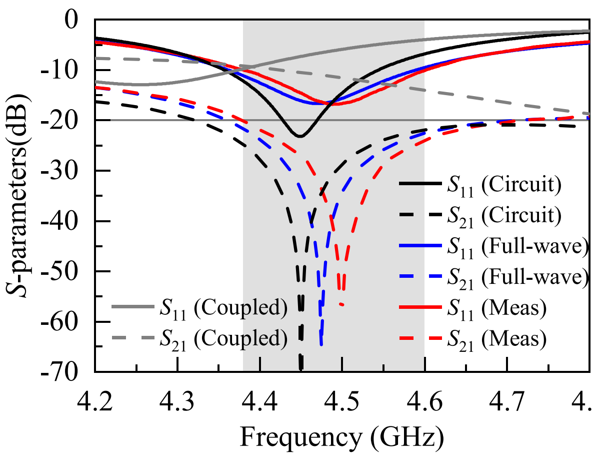

FIGURE 14. Calculated, simulated, and measured S-parameters of the proposed closely spaced MPAs and the coupled case.

only needs to make a minor fine-tune to 28.7 mm. The S-parameters and radiation performances are measured by the Rohde & Schwarz ZNB-20 Vector Network Analyzer and SATIMO measurement system, respectively.

Fig. 14 shows the S-parameters of the proposed closely spaced MPAs under the circuit model calculation, full-wave simulation, and measurement, respectively. As seen, the S_{21} under circuit model agrees very well with that of the full-wave simulation at only about 20 MHz (0.4%) deviation, showing a good prediction. Meanwhile, the measured results are also basically consistent with the simulation, only exhibiting a slight shifting due to the fabricated tolerances, demonstrating an impedance matching bandwidth range of $4.38 \sim 4.60$ GHz (4.9%) for $S_{11} < -10$ dB and an isolation bandwidth in a frequency range from $4.38 \sim 4.71$ GHz (7.33%) for $S_{21} < -20$ dB. Compared with the initial coupling of -7 dB, the maximum isolation is improved to 58 dB. The excellent isolation performance is achieved by such a simple decoupling structure as mainly attributed to the circuit-level prediction during the proposed design procedure.

The simulated and measured normalized radiation patterns of the decoupled MPAs at the center frequency, which are excited from port 1 and port 2, are shown in Fig. 15. The measured results are in good agreement with the simulated ones. In the E-plane, the radiation patterns of the two MPAs exhibit only a slight asymmetry, which is significantly improved compared to the coupled case. Besides, the measured front-to-back ratio (FBR) and the cross-polarization levels are 18 dB and 22 dB, respectively. In the H-plane, the radiation patterns of two elements are symmetric with an 18-dB FBR and a 20-dB cross- polarization level at the boresight direction. As shown in Fig. 16, the simulated and measured gain and total efficiency are basically in agreement, with slight differences fluctuating in the range of $0.1 \sim 0.9$ dBi and $0.05 \sim 0.1$, which comes from the inevitable fabrication and measurement tolerances. The measured total efficiency varies from 81.1% to 93.2% and the

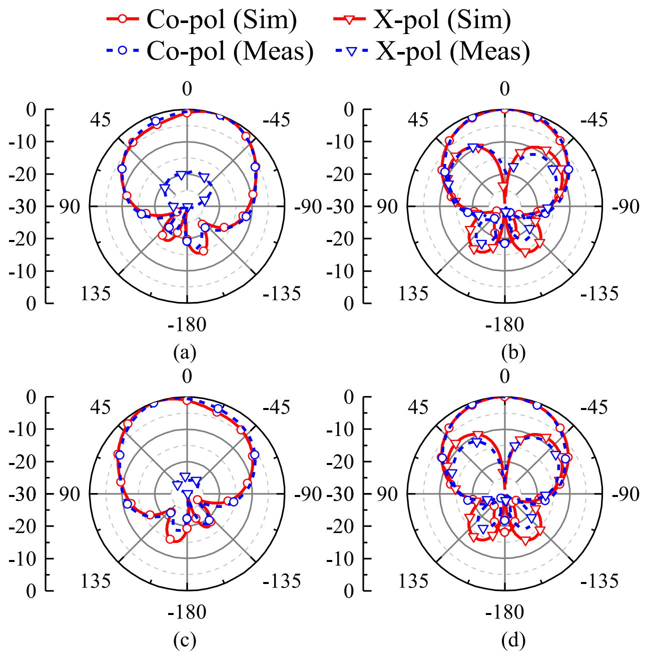

FIGURE 15. Simulated and measured radiation patterns of the proposed closely spaced MPAs in E-plane (*xoz* plane) and H-plane (*yoz* plane). (a) E-plane, and (b) H-plane radiation patterns for Port 1. (c) E-plane, and (d) H-plane radiation patterns for Port 2.

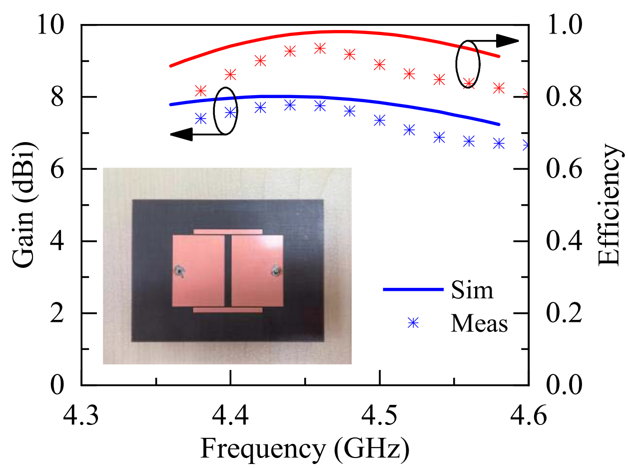

FIGURE 16. Simulated and measured gains and total efficiencies of the proposed closely spaced MPAs.

measured gain is from $7.0 \sim 7.8$ dBi in comparison to the simulated gain of $7.3 \sim 8.0$ dBi.

The ECC performances of the proposed antennas before and after using the decoupling structure within the operating bandwidth are depicted in Fig. 17. As seen, the simulated ECCs are significantly reduced from around 0.19 to 0.002 after the introduction of the decoupling structure, which is also in good agreement with the measured result.

B. COMPARISON

To highlight the merits of the proposed systematic decoupling method, a comprehensive comparison in design

TABLE 2. Comparison between the proposed and other reported works.

Ref.	Decoupling Methods	Systematic Design	ED / CD (λ_0)	Layers	Profile (λ_0)	10-dB IBW (%)	Ori. / Opt. Isolation (Improvement)	In-band Isolation (dB)	Gain (dBi)	Efficiency (%)
[4]	EBG	NO	0.22 / 0.5	1	0.02	2.5	16→30 (14)	> 30	/	/
[9]	Dielectric block	NO	0.027 / 0.10	2	0.18	27.3	9→30 (21)	> 20	4.1	87.4 ~ 97.2
[10]	Coupling-mode transducers	NO	0.024 / 0.57	2	0.09	5.8	9→37 (28)	> 20	4.7	67.0 ~ 74.0
[11]	DGS	NO	0.031 / 0.33	1	/	1.7	13→45 (32)	> 30	0.5	/
[12]	Meta-wall	NO	0.60 / 0.91	> 2	0.24	8.7	18→25 (7)	> 25	8.0	~ 84.6
[14]	DMN	YES	0.06 / 0.45	2	0.06	3.1	9→33 (22)	> 22	8.0	/
[16]	DMN	YES	0.345 / 0.65	2	0.20	5.3	24→58 (34)	> 28	6.5	/
[23]	CM / DM	YES	0.016 / 0.44	2	0.05	5.5	5→15.4 (10.4)	≈ 15.4	7.8	81.9 ~ 87.0
[26]	Two Paths (MSL with Pin)	NO	0.027 / 0.40	1	0.02	1.4	7→18 (11)	> 18	5.5	/
[27]	Two Paths (U-section MSL)	NO	0.29 / 0.60	1	0.077	4.9	23→33 (10)	> 30	7.7	/
This work	Two Paths (MSL)	YES	0.04 / 0.37	1	0.05	4.9	7→58 (51)	> 20	7.8	81.1 ~ 93.2

*ED: Edge-to-edge distance, CD: Center-to-center distance, MSL: Microstrip line, IBW: Impedance bandwidth.

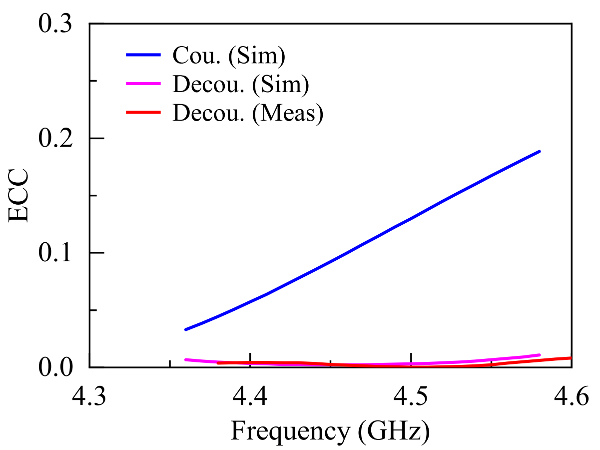

FIGURE 17. Simulated and measured ECCs with and without the decoupling structure.

methods, physical dimensions, isolation property, and radiation performance with recently relevant research is tabulated in Table 2. As discussed in Section I, a systematic design method is an urgent requirement for decoupling in closely spaced MPAs, with the benefit of offering a clear design guideline to reduce design complexity and provide performance prediction. Among the traditional decoupling methods, only the DMN method in [14] and [16] has the capability of systematic design but suffers from the multi-layer complex structures and sacrifices operating bandwidth. Here it specifically means that these antennas have a higher profile but similar or even lower operating bandwidth. The CM/DM method proposed in [23] provides a design guideline but cannot predict performance and can only minimize the isolation in a best-effort manner by sweeping the parameters, thus bearing limited in-band isolation. In an interesting work [43], exploiting the self-resonance frequency of the CM and DM can improve the prediction and evaluation ability of CM/DM method. Moreover, the traditional two-paths decoupling method used in [26] and [27] lacks design guidance and relies heavily on a try-and-error approach to design, which still suffers from limited operating bandwidth and decoupling capability.

In summary, the proposed systematic design method based on the two-path decoupling technique has demonstrated excellent performance in many aspects, especially in providing quantitative design guidance and isolation performance prediction. Meanwhile, better isolation performances have been achieved with a simpler decoupling structure, and the impedance matching bandwidth and radiation characteristics have been maintained similar to those of a single MPA. Moreover, the proposed design method has the ability applied in other antenna arrays to help improve decoupling design efficiency, and it can also be employed in broadband or multi-band decoupling designs by increasing the zeros [44].

V. CONCLUSION

This article presents a systematic design method to suppress the mutual coupling between closely spaced patch antennas.

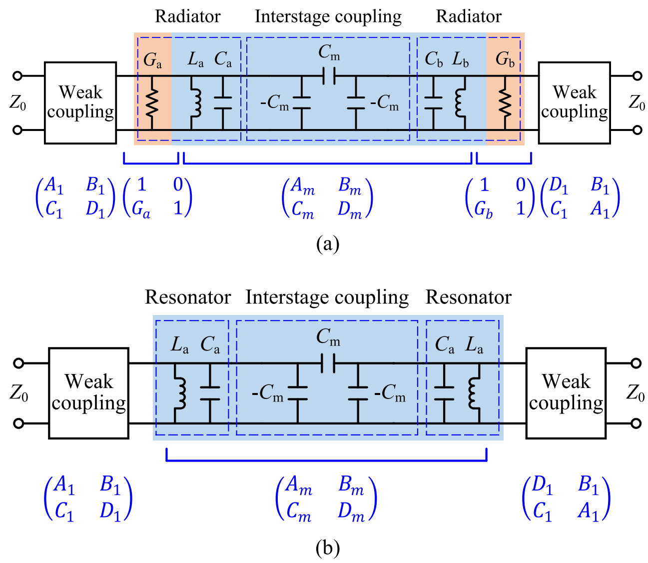

FIGURE 18. **Equivalent circuit model for extracting the coupling coefficients. (a) Lossy network. (b) Lossless network.**

Unlike traditional two-path cancellation methods that rely on trial and error to mitigate mutual coupling in a best- effort manner, the proposed scheme can provide a design guideline and predict the isolation performance. Due to the inability to separate the two paths at the antenna level and the original coupling path is difficult to analyze, the analysis at the circuit level is introduced. Based on a practical and simple structure, the conditions of isolation and impedance matching are then derived by accurate extraction and modeling to obtain the rigorous relationships between the lumped elements of the two paths. As such, the antenna-level implementation and quantitative design can be conveniently realized based on the circuit-level discussion. To validate the proposed method, a prototype is in final simulated, fabricated, and measured. The corresponding circuit-model calculation, full-wave simulation, and measurement of the specific two closely spaced MPAs agree well, thereby evidently demonstrating significant improvements in isolation characteristics, impedance matching, and radiation performance.

APPENDIX

The detailed derivations for extracting and calculating the coupling coefficient (*CC*) directly from the two radiating patches are presented in this section, which is inspired and based on the previous work [39]. The equivalent circuit model for extracting the *CC* is depicted in Fig. 18(a), where the parallel *GLC* circuits and the interstage coupling components are the same as those in Path A shown in Fig. 4, except that the external coupling at the ports is set to weak coupling. The network in Fig. 18(b) is the corresponding lossless network without the radiation conductance (G_a and G_b) of the two closely spaced radiating patches, and the rest of the lumped components are the same as in Fig. 18(a). It is well known that the *CC* can be directly extracted from the two steep peaks of the transmission responses in the lossless network. Therefore, as long as the relationship between the two networks is deduced, the *CC* can also be directly extracted from the lossy network in the same manner.

Firstly, the transmission response of the lossy network in Fig. 18(a) can be obtained by multiplying the five-part cascaded *A*-matrices, such that

$$\begin{pmatrix} A_R & B_R \\ C_R & D_R \end{pmatrix} = \begin{pmatrix} A_1 & B_1 \\ C_1 & D_1 \end{pmatrix} \begin{pmatrix} 1 & 0 \\ G_a & 1 \end{pmatrix} \begin{pmatrix} A_m & B_m \\ C_m & D_m \end{pmatrix} \begin{pmatrix} 1 & 0 \\ G_b & 1 \end{pmatrix} \begin{pmatrix} D_1 & B_1 \\ C_1 & A_1 \end{pmatrix} \tag{7a}$$

where A_R, B_R, C_R, and D_R are given by (7b), shown at the bottom of the page.

Then, the transmission matrix of the lossless network without G_a and G_b can be expressed as

$$\begin{pmatrix} A'_R & B'_R \\ C'_R & D'_R \end{pmatrix} = \begin{pmatrix} A_1 & B_1 \\ C_1 & D_1 \end{pmatrix} \begin{pmatrix} A_m & B_m \\ C_m & D_m \end{pmatrix} \begin{pmatrix} D_1 & B_1 \\ C_1 & A_1 \end{pmatrix} \tag{8a}$$

where the elements of this matrix are given by

$$\begin{cases} A'_R = A_1 B_m C_1 + A_1 A_m D_1 + B_1 C_m D_1 + B_1 C_1 D_m \\ B'_R = {A_1}^2 B_m + {B_1}^2 C_m + A_1 B_1 (A_m + D_m) \\ C'_R = B_m {C_1}^2 + D_1 (C_m D_1 + C_1 (A_m + D_m)) \\ D'_R = A_m B_1 C_1 + A_1 B_m C_1 + B_1 C_m D_1 + A_1 D_1 D_m \end{cases} \tag{8b}$$

It can be seen that the terms in (8b) are exactly all the terms in (7b) of the lossy network that excludes G_a and G_b. Obviously, the lossy terms must be eliminated if one would like to extract directly from the lossy network. For the lossless parts of the lossy network, A and D in the ABCD matrix are pure real quantities, while B and C are pure imaginary quantities. More specifically, the weak coupling can be simply represented by an admittance inverter, such that

$$\begin{pmatrix} A_1 & B_1 \\ C_1 & D_1 \end{pmatrix} = \begin{pmatrix} 0 & -j/J_1 \\ -jJ_1 & 0 \end{pmatrix} \tag{9}$$

where J_1 is the value of the *J*-inverter.

The matrix of the middle part is obtained by multiplying the corresponding cascaded component matrices, which is given by

$$\begin{pmatrix} A_m & B_m \\ C_m & D_m \end{pmatrix} = \begin{pmatrix} 1 & 0 \\ j\omega C_a + 1/(j\omega L_a) & 1 \end{pmatrix} \cdot \begin{pmatrix} 0 & -j/(\omega C_m) \\ -j\omega C_m & 0 \end{pmatrix} \cdot \begin{pmatrix} 1 & 0 \\ j\omega C_b + 1/(j\omega L_b) & 1 \end{pmatrix} \tag{10}$$

$$\begin{cases} A_R = A_1 B_m C_1 + A_1 A_m D_1 + B_1 C_m D_1 + B_1 C_1 D_m + A_1 B_m D_1 G_b + B_1 B_m C_1 G_a + B_1 D_1 (A_m G_a + D_m G_b) + B_1 B_m D_1 G_a G_b \\ B_R = {A_1}^2 B_m + {B_1}^2 C_m + A_1 B_1 (A_m + D_m) + B_1 (A_m B_1 G_a + B_1 D_m G_b + A_1 B_m (G_a + G_b)) + {B_1}^2 B_m G_a G_b \\ C_R = B_m {C_1}^2 + D_1 (C_m D_1 + C_1 (A_m + D_m)) + D_1 (B_m C_1 (G_a + G_b) + D_1 (A_m G_a + D_m G_b)) + B_m {D_1}^2 G_a G_b \\ D_R = A_m B_1 C_1 + A_1 B_m C_1 + B_1 C_m D_1 + A_1 D_1 D_m + A_m B_1 D_1 G_a + A_1 B_m D_1 G_a + B_1 (B_m C_1 + D_1 D_m) G_b + B_1 B_m D_1 G_a G_b \end{cases} \tag{7b}$$

Therefore, the relationship between the lossless and the lossy matrices can be simplified and derived as

$$\begin{cases} A'_R = \mathrm{Re}(A_R) \\ B'_R = j\left(\mathrm{Im}(B_R) + \frac{G_a G_b}{\omega C_m {J_1}^2}\right) \\ C'_R = j\mathrm{Im}(C_R) \\ D'_R = \mathrm{Re}(D_R) \end{cases} \tag{11}$$

Unfortunately, G_a and G_b are still present in B'_R and cannot be ignored. Interestingly, if the A-matrix of the lossless network is converted into a Z-matrix, it can be found that only $Z'_{\mathrm{R}12}$ includes B'_R. Since this network is reciprocal, that is, $Z'_{\mathrm{R}12} = Z'_{\mathrm{R}21}$, the term of $Z'_{\mathrm{R}12}$ could be replaced by $Z'_{\mathrm{R}21}$, and the Z-matrix can be substituted into (11) and deduced as

$$Z'_R = \begin{pmatrix} \frac{A'_R}{C'_R} & \frac{A'_R D'_R - B'_R C'_R}{C'_R} \\ \frac{1}{C'_R} & \frac{D'_R}{C'_R} \end{pmatrix} = \begin{pmatrix} \frac{\mathrm{Re}(A_R)}{j\mathrm{Im}(C_R)} & \frac{1}{j\mathrm{Im}(C_R)} \\ \frac{1}{j\mathrm{Im}(C_R)} & \frac{\mathrm{Re}(D_R)}{j\mathrm{Im}(C_R)} \end{pmatrix} \tag{12}$$

Finally, the transmission response in the lossy network with no effect from radiation conductance can be expressed as

$$S'_{21} = \frac{\frac{2Z_0}{j\mathrm{Im}(C_R)}}{\left(\frac{\mathrm{Re}(A_R)}{j\mathrm{Im}(C_R)} + Z_0\right)\left(\frac{\mathrm{Re}(D_R)}{j\mathrm{Im}(C_R)} + Z_0\right) + \frac{1}{Im^2(C_R)}} \tag{13}$$

where Z_0 is the port impedance.

As shown in Fig. 5, the transmission response (denoted by the red line) extracted directly from the network including radiation loss by using (13) exhibits two significant steep peaks compared to the original response (denoted by the blue line), which are consistent with the two steep peaks extracted from the lossless network (denoted by the black dashed line). Now, the *CC* between the two radiating patches can be readily and accurately determined by substituting the two extracted frequencies into the following equation in final.

$$CC = \frac{1}{2}\left(\frac{f_b}{f_a} + \frac{f_a}{f_b}\right)\sqrt{\left(\frac{{f_2}^2 - {f_1}^2}{{f_2}^2 + {f_1}^2}\right)^2 - \left(\frac{{f_b}^2 - {f_a}^2}{{f_b}^2 + {f_a}^2}\right)^2} \tag{14}$$

where f_a and f_b are the self-resonant frequencies of the two patch antennas, f_1 and f_2 are the characteristic frequencies resulting from the patch coupling.

ACKNOWLEDGMENT
The authors are indebted to Dr. Qiong-Sen Wu from Guangdong University of Technology, Guangzhou, China, for his beneficial discussions on this work.

REFERENCES
[1] M. A. Jensen and J. W. Wallace, "A review of antennas and propagation for MIMO wireless communications," *IEEE Trans. Antennas Propag.*, vol. 52, no. 11, pp. 2810–2824, Nov. 2004.
[2] J. H. Winters, "On the capacity of radio communication systems with diversity in a Rayleigh fading environment," *IEEE J. Sel. Areas Commun.*, vol. SAC-5, no. 5, pp. 871–878, Jun. 1987.
[3] T. Svantesson and A. Ranheim, "Mutual coupling effects on the capacity of multielement antenna systems," in *Proc. IEEE Int. Conf. Acoust., Speech, Signal Process.*, vol. 4, May 2001, pp. 2485–2488.
[4] X. Yang, Y. Liu, Y.-X. Xu, and S. Gong, "Isolation enhancement in patch antenna array with fractal UC-EBG structure and cross slot," *IEEE Antennas Wireless Propag. Lett.*, vol. 16, pp. 2175–2178, 2017.
[5] H. S. Farahani, M. Veysi, M. Kamyab, and A. Tadjalli, "Mutual coupling reduction in patch antenna arrays using a UC-EBG superstrate," *IEEE Antennas Wireless Propag. Lett.*, vol. 9, pp. 57–59, 2010.
[6] F. Yang and Y. Rahmat-Samii, "Microstrip antennas integrated with electromagnetic band-gap (EBG) structures: A low mutual coupling design for array applications," *IEEE Trans. Antennas Propag.*, vol. 51, no. 10, pp. 2936–2946, Oct. 2003.
[7] A. Habashi, J. Nourinia, and C. Ghobadi, "Mutual coupling reduction between very closely spaced patch antennas using low-profile folded split-ring resonators (FSRRs)," *IEEE Antennas Wireless Propag. Lett.*, vol. 10, pp. 862–865, 2011.
[8] Y.-F. Cheng, X. Ding, W. Shao, and B.-Z. Wang, "Reduction of mutual coupling between patch antennas using a polarization-conversion isolator," *IEEE Antennas Wireless Propag. Lett.*, vol. 16, pp. 1257–1260, 2017.
[9] M. Li, M. Y. Jamal, L. Jiang, and K. L. Yeung, "Isolation enhancement for MIMO patch antennas sharing a common thick substrate: Using a dielectric block to control space-wave coupling to cancel surface-wave coupling," *IEEE Trans. Antennas Propag.*, vol. 69, no. 4, pp. 1853–1863, Apr. 2021.
[10] M. Li, B. G. Zhong, and S. W. Cheung, "Isolation enhancement for MIMO patch antennas using near-field resonators as coupling-mode transducers," *IEEE Trans. Antennas Propag.*, vol. 67, no. 2, pp. 755–764, Feb. 2019.
[11] J. OuYang, F. Yang, and Z. M. Wang, "Reducing mutual coupling of closely spaced microstrip MIMO antennas for WLAN application," *IEEE Antennas Wireless Propag. Lett.*, vol. 10, pp. 310–313, 2011.
[12] M.-C. Tang et al., "Mutual coupling reduction using meta-structures for wideband, dual-polarized, and high-density patch arrays," *IEEE Trans. Antennas Propag.*, vol. 65, no. 8, pp. 3986–3998, Aug. 2017.
[13] H. Qi, L. Liu, X. Yin, H. Zhao, and W. J. Kulesza, "Mutual coupling suppression between two closely spaced microstrip antennas with an asymmetrical coplanar strip wall," *IEEE Antennas Wireless Propag. Lett.*, vol. 15, pp. 191–194, 2016.
[14] X.-J. Zou, G.-M. Wang, Y.-W. Wang, and H.-P. Li, "An efficient decoupling network between feeding points for multielement linear arrays," *IEEE Trans. Antennas Propag.*, vol. 67, no. 5, pp. 3101–3108, May 2019.
[15] Y.-M. Zhang, S. Zhang, J.-L. Li, and G. F. Pedersen, "A transmission-line-based decoupling method for MIMO antenna arrays," *IEEE Trans. Antennas Propag.*, vol. 67, no. 5, pp. 3117–3131, May 2019.
[16] R.-L. Xia, S.-W. Qu, P.-F. Li, Q. Jiang, and Z.-P. Nie, "An efficient decoupling feeding network for microstrip antenna array," *IEEE Antennas Wireless Propag. Lett.*, vol. 14, pp. 871–874, 2015.
[17] C. Volmer, J. Weber, R. Stephan, K. Blau, and M. A. Hein, "An Eigen-analysis of compact antenna arrays and its application to port decoupling," *IEEE Trans. Antennas Propag.*, vol. 56, no. 2, pp. 360–370, Feb. 2008.
[18] M. Li, S. Tian, M.-C. Tang, and L. Zhu, "A compact low-profile hybrid-mode patch antenna with intrinsically combined self-decoupling and filtering properties," *IEEE Trans. Antennas Propag.*, vol. 70, no. 2, pp. 1511–1516, Feb. 2022.
[19] Q. X. Lai, Y. M. Pan, S. Y. Zheng, and W. J. Yang, "Mutual coupling reduction in MIMO microstrip patch array using TM_{10} and TM_{02} modes," *IEEE Trans. Antennas Propag.*, vol. 69, no. 11, pp. 7562–7571, Nov. 2021.
[20] H. Deng, L. Zhu, N.-W. Liu, and J.-F. Lin, "Co-linear polarization decoupling of two feeding ports in a single patch antenna without radiation patterns deterioration," *Int. J. RF Microw. Comput. Eng.*, vol. 32, no. 2, pp. 1–15, Feb. 2022.
[21] H.-W. Lin, Q. Chen, Y. Ji, X. Yang, J. Wang, and L. Ge, "Weak-field-based self-decoupling patch antennas," *IEEE Trans. Antennas Propag.*, vol. 68, no. 6, pp. 4208–4217, Jun. 2020.
[22] J.-F. Lin, H. Deng, and L. Zhu, "Design of low profile compact MIMO antenna on a single radiating patch using simple and systematic characteristic modes method," *IEEE Trans. Antennas Propag.*, vol. 70, no. 3, pp. 1612–1622, Mar. 2022.
[23] L.-B. Sun, Y. Li, and Z. Zhang, "Decoupling between extremely closely spaced patch antennas by mode cancellation method," *IEEE Trans. Antennas Propag.*, vol. 69, no. 6, pp. 3074–3083, Jun. 2021.

[24] X.-D. Mei and K.-L. Wu, "How low does mutual coupling need to be for MIMO antennas," in *Proc. IEEE AP-S Antennas Propag. Symp.*, Jul. 2018, pp. 1579–1580.
[25] X. Chen, S. Zhang, and Q. Li, "A review of mutual coupling in MIMO systems," *IEEE Access*, vol. 6, pp. 24706–24719, 2018.
[26] T. Pei, L. Zhu, J. Wang, and W. Wu, "A low-profile decoupling structure for mutual coupling suppression in MIMO patch antenna," *IEEE Trans. Antennas Propag.*, vol. 69, no. 10, pp. 6145–6153, Oct. 2021.
[27] S. Farsi, H. Aliakbarian, D. Schreurs, B. Nauwelaers, and G. A. E. Vandenbosch, "Mutual coupling reduction between planar antennas by using a simple microstrip U-section," *IEEE Antennas Wireless Propag. Lett.*, vol. 11, pp. 1501–1503, 2012.
[28] K.-L. Wu, C. Wei, X. Mei, and Z.-Y. Zhang, "Array-antenna decoupling surface," *IEEE Trans. Antennas Propag.*, vol. 65, no. 12, pp. 6728–6738, Dec. 2017.
[29] S. Ranvier et al., "Mutual coupling reduction for patch antenna array," in *Proc. 1st Eur. Conf. Antennas Propag.*, Nov. 2006, pp. 209–210.
[30] M. Troubat et al., "Mutual synthesis of combined microwave circuits applied to the design of a filter-antenna subsystem," *IEEE Trans. Microw. Theory Techn.*, vol. 55, no. 6, pp. 1182–1189, Jun. 2007.
[31] J. Sui and K.-L. Wu, "A self-decoupled antenna array using inductive and capacitive couplings cancellation," *IEEE Trans. Antennas Propag.*, vol. 68, no. 7, pp. 5289–5296, Jul. 2020.
[32] R. Zaker and A. Kheirdoost, "Bandwidth and isolation improvement of highly coupled printed array antenna using multiple shorting posts," *IEEE Trans. Antennas Propag.*, vol. 69, no. 11, pp. 7987–7992, Nov. 2021.
[33] C.-Y. Chiu, F. Xu, S. Shen, and R. D. Murch, "Mutual coupling reduction of rotationally symmetric multiport antennas," *IEEE Trans. Antennas Propag.*, vol. 66, no. 10, pp. 5013–5021, Oct. 2018.
[34] R. Garg, P. Bhartia, I. Bahl, and A. Ittipiboon, *Microstrip Antenna Design Handbook*. Norwood, MA, USA: Artech House, 2001.
[35] Z. H. Jiang and D. H. Werner, "A compact, wideband circularly polarized co-designed filtering antenna and its application for wearable devices with low SAR," *IEEE Trans. Antennas Propag.*, vol. 63, no. 9, pp. 3808–3818, Sep. 2015.
[36] J.-S. Hong and M. J. Lancaster, *Microstrip Filters for RF/Microwave Applications*, 2nd ed. Hoboken, NJ, USA: Wiley, 2011.
[37] J.-F. Lin and Q.-X. Chu, "Accurately characterizing the coupling effects of patch antennas with complex- and frequency-dependent J/K inverters," *IEEE Trans. Antennas Propag.*, vol. 67, no. 3, pp. 1554–1561, Mar. 2019.
[38] K. C. Gupta, R. Garg, and I. J. Bahl, *Microstrip Lines and Slotlines*. Dedham, MA, USA: Artech House, 1979.
[39] Q.-S. Wu, X. Zhang, and L. Zhu, "An improved method for accurate extraction of coupling coefficient between a lossy radiator and a lossless resonator in filtering antennas," *IEEE Access*, vol. 6, pp. 39927–39935, 2018.
[40] S. Zhang and L. Zhu, "Synthesis method for even-order symmetrical Chebyshev bandpass filters with alternative J/K inverters and lambda/4 resonators," *IEEE Trans. Microw. Theory Techn.*, vol. 61, no. 2, pp. 808–816, Feb. 2013.
[41] Q.-X. Chu and H. Wang, "A compact open-loop filter with mixed electric and magnetic coupling," *IEEE Trans. Microw. Theory Techn.*, vol. 56, no. 2, pp. 431–439, Feb. 2008.
[42] D. R. Jackson and N. G. Alexopoulos, "Simple approximate formulas for input resistance, bandwidth, and efficiency of a resonant rectangular patch," *IEEE Trans. Antennas Propag.*, vol. 39, no. 3, pp. 407–410, Mar. 1991.
[43] A. Zhao and Z. Ren, "Antenna decoupling based on self-resonance frequencies of common mode and differential mode," *IEEE Access*, vol. 9, pp. 145763–145773, 2021.
[44] H. Deng and L. Zhu, "Self-decoupled dual-frequency patch antennas via hybrid coupling interface technique," *IEEE Antennas Wireless Propag. Lett.*, early access, Jan. 24, 2023, doi: 10.1109/LAWP.2023.3239380.

HUI DENG (Graduate Student Member, IEEE) was born in Hunan, China, in 1993. He received the B.Eng. and M.Eng. degrees in electronic engineering from the University of Electronic Science and Technology of China, Chengdu, China, in 2016 and 2019, respectively. He is currently pursuing the Ph.D. degree with the Faculty of Science and Technology, University of Macau, Macau, SAR, China.

His current research interests include antenna decoupling and the design of MIMO antennas. He was a recipient of the Best Student Paper Award from the 2022 IEEE MTT-S International Microwave Workshop Series on Advanced Materials and Processes for RF and THz Applications.

LEI ZHU (Fellow, IEEE) received the B.Eng. and M.Eng. degrees in radio engineering from the Nanjing Institute of Technology (currently, Southeast University), Nanjing, China, in 1985 and 1988, respectively, and the Ph.D. degree in electronic engineering from the University of Electro-Communications, Tokyo, Japan, in 1993.

He was a Research Engineer with Matsushita-Kotobuki Electronics Industries Ltd., Tokyo, from 1993 to 1996, a Research Fellow with the École Polytechnique de Montréal, Montreal, QC, Canada, from 1996 to 2000, and an Associate Professor with the School of Electrical and Electronic Engineering, Nanyang Technological University, Singapore, from 2000 to 2013. He joined the Faculty of Science and Technology, University of Macau, Macau, China, as a Full Professor in August 2013, and has been a Distinguished Professor since December 2016. From August 2014 to August 2017, he served as the Head of the Department of Electrical and Computer Engineering, University of Macau. So far, he has authored or coauthored more than 750 papers in international journals and conference proceedings. His papers have been cited more than 15 000 times with the H-index of 61 (source: Scopus). His research interests include microwave circuits, antennas, periodic structures, and computational electromagnetics.

Dr. Zhu was the recipient of the 1993 Achievement Award in Science and Technology (First Prize) from the National Education Committee of China, the 1996 Silver Award of Excellent Invention from Matsushita-Kotobuki Electronics Industries Ltd., the 1997 Asia–Pacific Microwave Prize Award, the 2020 FST Research Excellence Award from the University of Macau, and the 2020 and 2022 Macao Natural Science Awards (Second Prize) from the Science and Technology Development Fund, Macau. He was an Associate Editor for the IEEE TRANSACTIONS ON MICROWAVE THEORY AND TECHNIQUES from 2010 to 2013 and IEEE MICROWAVE AND WIRELESS COMPONENTS LETTERS from 2006 to 2012. He served as the General Chair for the 2008 IEEE MTT-S International Microwave Workshop Series on the Art of Miniaturizing RF and Microwave Passive Components, Chengdu, China, and a Technical Program Committee Co-Chair of the 2009 Asia–Pacific Microwave Conference, Singapore. He served as the member of IEEE MTT-S Fellow Evaluation Committee from 2013 to 2015, and the IEEE AP-S Fellows Committee from 2015 to 2017.

ZHAO-AN OUYANG (Member, IEEE) was born in Guangzhou, China, in 1990. He received the B.Eng. and M.Eng. degrees from the South China University of Technology, Guangzhou, in 2013 and 2016, respectively, and the Ph.D. degree from the University of Macau, Macau, SAR, China, in 2022.

He was a Research Fellow with the University of Macau from February 2022 to August 2022. He has been as a Lecturer with the College of Information Science and Technology, Jinan University, Guangzhou, China, since September 2022. His current research interests include the design of planar balanced filters and microwave circuits. He was a recipient of the Best Student Paper Award from the 2020 International Conference on Microwave and Millimeter Wave Technology.